

Submitted to ApJ

Monte Carlo Simulation of Ly α Scattering and Application to Damped Ly α Systems

Zheng Zheng & Jordi Miralda-Escudé

Department of Astronomy, The Ohio State University, 140 West 18th Avenue, Columbus, OH 43210, USA

`zhengz@astronomy.ohio-state.edu, jordi@astronomy.ohio-state.edu`

ABSTRACT

A Monte Carlo code to solve the transfer of Ly α photons is developed, which can predict the Ly α image and two-dimensional Ly α spectra of a hydrogen cloud with any given geometry, Ly α emissivity, neutral hydrogen density distribution, and bulk velocity field. We apply the code to several simple cases of a uniform cloud to show how the Ly α image and emitted line spectrum is affected by the column density, internal velocity gradients, and emissivity distribution. We then apply the code to two models for damped Ly α absorption systems: a spherical, static, isothermal cloud, and a flattened, axially symmetric, rotating cloud. If the emission is due to fluorescence of the external background radiation, the Ly α image should have a core corresponding to the region where hydrogen is self-shielded. The emission line profile has the characteristic double peak with a deep central trough. We show how rotation of the cloud causes the two peaks to shift in wavelength as the slit is perpendicular to the rotation axis, and how the relative amplitude of the two peaks is changed. In reality, damped Ly α systems are likely to have a clumpy gas distribution with turbulent velocity fields, which should smooth the line emission profile, but should still leave the rotation signature of the wavelength shift across the system.

Subject headings: line:formation – radiative transfer – scattering – quasars: absorption lines

1. Introduction

The high column density absorption systems (damped Ly α and Lyman limit systems) are a key part of understanding galaxy formation. As a galaxy collapses from the highly ionized intergalactic medium, the gas will inevitably go through a phase of a self-shielded cloud of atomic hydrogen before it can cool and collapse further into molecular clouds, form stars, and increase its metallicity. Many

of the damped Ly α systems (DLAs) at high redshift may be gaseous halos in the process of forming galaxies rather than fully formed spiral disks, especially in view of the very low metallicities at high redshifts (Lu et al. 1996; Prochaska, Gawiser, & Wolfe 2001). If so, the internal structure of these objects should reveal to us the detailed processes by which galaxies form. Several basic questions arise in relation to this: how big are the absorption systems? Is the gas smoothly distributed, or is it in the form of clumps and an interclump medium? If so, how big are the clumps? What is the dynamical state of the gas? How does its mean rotation velocity compare to its velocity dispersion?

Some of these questions may be addressed by studying the associated metal absorption lines (e.g., Prochaska & Wolfe 1997, 1998) or by radio and optical observations of galaxies found to be associated with the absorbers (see Briggs et al. 1989; Djorgovski et al. 1996), although the majority of DLAs at high redshifts might not be associated with luminous galaxies.

An alternative observational probe of the structure of DLA and Lyman limit systems may be found in their Ly α emission produced in hydrogen recombinations and the subsequent scattering of Ly α photons through the gas (Hogan & Weymann 1987; Gould & Weinberg 1996). The source of the ionization may be the external cosmic ionizing radiation, shock-heating due to the gravitational collapse of the gas in a dark matter halo, or star formation within the system. In the case of fluorescence of external radiation, the maximum surface brightness is achieved in any system with $N_{HI} \gtrsim 10^{18} \text{ cm}^{-2}$, where all the incident external photons are absorbed.

Hydrogen Ly α line is a resonance line. The problem of radiative transfer of resonance line radiation can be approximately solved analytically under certain conditions (e.g., Harrington 1973, 1974; Neufeld 1990). These analytic solutions can be found only for a limited number of cases such as a static, extremely opaque and plane-parallel medium. In some cases, numerical methods are used to solve the transfer equation exactly (e.g., Adams 1972; Hummer & Kunasz 1980). For a more general geometry, density distribution, and kinematics, Monte Carlo simulations can be very useful (Bonilhá et al. 1979; Ahn, Lee, & Lee 2000, 2001, 2002).

This paper presents the results of a numerical Monte Carlo code we have developed to compute the transfer of Ly α photons through an arbitrary distribution of hydrogen. The code predicts the two-dimensional (2-D) image and line-spectrum along any given observed direction, for a general three-dimensional distribution of gas of given geometry, Ly α emissivity, neutral hydrogen density, and bulk velocity field. In this paper, it will be applied only to spherical and axially symmetric clouds, although in the future it can be applied to results of numerical simulations of galaxy formation.

We describe the Monte Carlo code in §2. In §3, we apply the code to several simple cases of hydrogen clouds to demonstrate the effects of the neutral hydrogen column density, Ly α emissivity and bulk velocity field on the spectra of escaped Ly α photons. In §4, we model DLAs as static and rotating clouds and investigate their 2-D Ly α emission spectra. Finally, we have a brief summary and discussion in §5.

2. Monte Carlo Simulation of Ly α Scattering

The method used to numerically compute the images and spectra of Ly α emission consists of generating random realizations of the trajectory of a large number of Ly α photons as they are scattered within the specified gas distribution. The first step is to generate the creation of the photon, with an emissivity distribution that depends on the model chosen. Next, an optical depth τ satisfying the exponential distribution is generated, and the spatial location at this optical depth along a randomly chosen direction of emission is found. We then choose the velocity of the atom that scatters the photon at this location, compute the new frequency of the photon after scattering, and generate the new direction of the photon. This process is repeated until the photon escapes the modeled system.

As these random realizations of photon trajectories are being carried out, a Ly α image of the system along a specified direction can be created. The image consists of a three-dimensional array of the two projected coordinates perpendicular to the direction of the image, and the frequency of the escaped photons, which contains the mean number of photons emitted at every projected position and frequency. At every scattering of a photon, the probability that the photon is re-emitted in the direction of the image and escapes is separately calculated. This probability is added on the element of the image array corresponding to the projected position and frequency of the photon (in practice, for the majority of the scatterings the optical depth is large and the probability of escape is negligible, so one can avoid the computation of the integral to obtain the optical depth in the direction of the image on most scatterings).

We now describe how the opacity of the Ly α photons is computed and the velocity of the atom at each scattering is generated. The scattering cross section of Ly α photons as a function of the frequency in the rest frame of the hydrogen atom is

$$\sigma_\nu = f_{12} \frac{\pi e^2}{m_e c} \frac{\Delta\nu_L/2\pi}{(\nu - \nu_0)^2 + (\Delta\nu_L/2)^2} , \quad (1)$$

where $f_{12} = 0.4162$ is the Ly α oscillator strength, $\nu_0 = 2.466 \times 10^{15}$ Hz is the line center frequency, $\Delta\nu_L = 4.03 \times 10^{-8} \nu_0 = 9.936 \times 10^7$ Hz is the natural line width, and the other symbols have their usual meaning. For a hydrogen atom with a component of velocity v_z along the photon's direction in a fixed “laboratory” frame, the term $\nu - \nu_0$ in the above equation becomes $(\nu_i - \nu_0) - (v_z/c)\nu_0$, where ν_i is the frequency of the incident photon in the “laboratory” frame. For a Maxwellian distribution of atom velocities, the resulting average cross section is

$$\sigma(x_i) = f_{12} \frac{\sqrt{\pi} e^2}{m_e c \Delta\nu_D} H(a, x_i) , \quad (2)$$

where

$$H(a, x) = \frac{a}{\pi} \int_{-\infty}^{+\infty} \frac{e^{-y^2}}{(x - y)^2 + a^2} dy \quad (3)$$

is the Voigt function, $\Delta\nu_D = (v_p/c) \nu_0$ is the Doppler frequency width, $v_p = (2kT/m_H)^{1/2}$ is the atom velocity dispersion times $\sqrt{2}$, T is the gas temperature, m_H is the hydrogen mass, $x_i =$

$(\nu_i - \nu_0)/\Delta\nu_D$ is the relative frequency of the incident photon in the laboratory frame, and $a = \Delta\nu_L/(2\Delta\nu_D)$ is the relative line width. The optical depth along the photon trajectory is computed by integrating the cross section in equation (2) times the atomic hydrogen density.

Once a spatial location where the photon is scattered has been chosen, the velocity v_z along the direction of the incident photon of the atom responsible for the scattering obeys the following distribution:

$$f(u_z) = \frac{a}{\pi} \frac{e^{-u_z^2}}{(x_i - u_z)^2 + a^2} H^{-1}(a, x_i), \quad (4)$$

where $u_z = v_z/v_p$. The two velocity components perpendicular to the direction of the photon simply follow a Gaussian distribution parameterized by the local temperature. To generate u_z with the distribution of equation (4), we generate first u_z with the distribution $g(u_z) \propto [(x_i - u_z)^2 + a^2]^{-1}$, which can be integrated and inverted analytically, and then keep the obtained value only if a second random number uniformly distributed between 0 and 1 is smaller than $e^{-u_z^2}$. In practice, when $|x_i| \gg 1$, this method is inefficient because a very small fraction of values of u_z are not discarded. So we use a trick to increase the fraction of acceptance. For $x_i > 0$, the comparison distribution $g(u_z)$ is modified by multiplying it by a factor $e^{-u_0^2}$ for $u_z > u_0$ and renormalizing it to a total probability of unity [for $x_i < 0$, we make use of the symmetry of $f(u_z)$ under the transformation of $x_i \rightarrow -x_i$ and $u_z \rightarrow -u_z$]. The value of u_0 can be chosen to minimize the fraction of generated values that will be discarded. The acceptance fractions are then required to be $e^{-u_z^2}$ and $e^{-u_z^2}/e^{-u_0^2}$ in the regions $u_z < u_0$ and $u_z > u_0$, respectively. A first random number uniformly distributed between 0 and 1 determines which region we use according to the modified $g(u_z)$ and a second random number determines whether the generated value of u_z is accepted by comparing it with the corresponding fraction of acceptance.

After the velocity of the atom is determined, the direction and frequency of the photon is first transformed to the rest frame of the atom. The direction of the scattered photon is then generated according to a dipole distribution. Its frequency differs from the incident one by the recoil effect, which is negligibly small in the applications we will present in this paper. The scattered photon is then transformed back to the laboratory frame, a new optical depth is chosen, and the entire process is repeated. In the presence of a fluid velocity, the procedure changes only by replacing the incident frequency x_i in equations (2) and (4) by its value in the fluid frame, $x_{fi} = x_i - (v_{fz}/c)(\nu_0/\Delta\nu_D)$, where v_{fz} is the fluid velocity parallel to the photon's direction (valid in the non-relativistic regime).

As mentioned previously, the Ly α image and spectrum of the system are calculated as the photon trajectories are randomly generated. At every photon scattering, we compute first the optical depth for the photon to escape the cloud along the direction of the image, and the photon is added to the corresponding element of the image array in projected position and frequency, with the weight $e^{-\tau}(1 + \mu^2)d\Omega$, where τ is the optical depth for escaping and μ is the cosine of the angle between the incident photon and the image direction (both μ and $d\Omega$ are measured in the rest frame of the atom). The factor $1 + \mu^2$ accounts for the dipole probability distribution of the direction of the photon after scattering. At the creation, a photon also has a probability to directly escape the

system along the direction of the image which is added to the corresponding element of the image array as well. After the contribution to the image has been done, a random direction of the new scattered photon is generated according to the same dipole distribution, and the realization of the photon trajectory is continued.

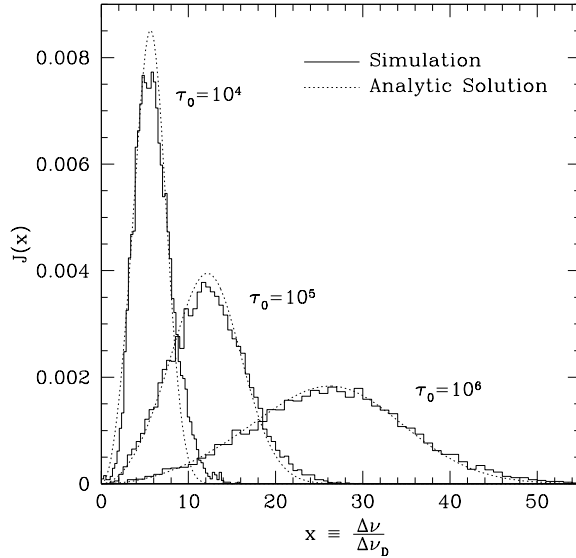


Fig. 1.— Comparison between results from our Monte Carlo simulations and the analytic solutions. The dotted lines are the analytic solutions (Neufeld 1990) of the Ly α spectra at one boundary of a slab with a midplane source and different scattering optical depths. The solid lines are those from simulations.

We test our numerical code for the case of a static, plane-parallel slab, for which Neufeld (1990) derived an analytic solution of the mean intensity in the limit of a large optical depth. We simulate the case of a midplane source radiating line-center Ly α photons in a plane-parallel slab of uniform density for three optical depths: $\tau_0 = 10^4, 10^5$, and 10^6 , where $\tau_0 = \sigma(x_i = 0)N_{HI}$ is the line-center optical depth from the midplane to the boundary of the slab. We assume a temperature $T = 10K$. We compare the spectra of the escaped Ly α photons with the analytic results (eq. 2.24 in Neufeld 1990; note that his definition of τ_0 differs from ours by a factor of $\sqrt{\pi}$. See also Ahn, Lee, & Lee 2001). Figure 1 shows excellent agreement, becoming better as the optical depth increases as expected since the analytic solution applies in the limit of a large optical depth.

3. Spherical Clouds of Uniform Density

We start applying our code to the most simple case of spherical hydrogen clouds with uniform density. We consider the following cases:

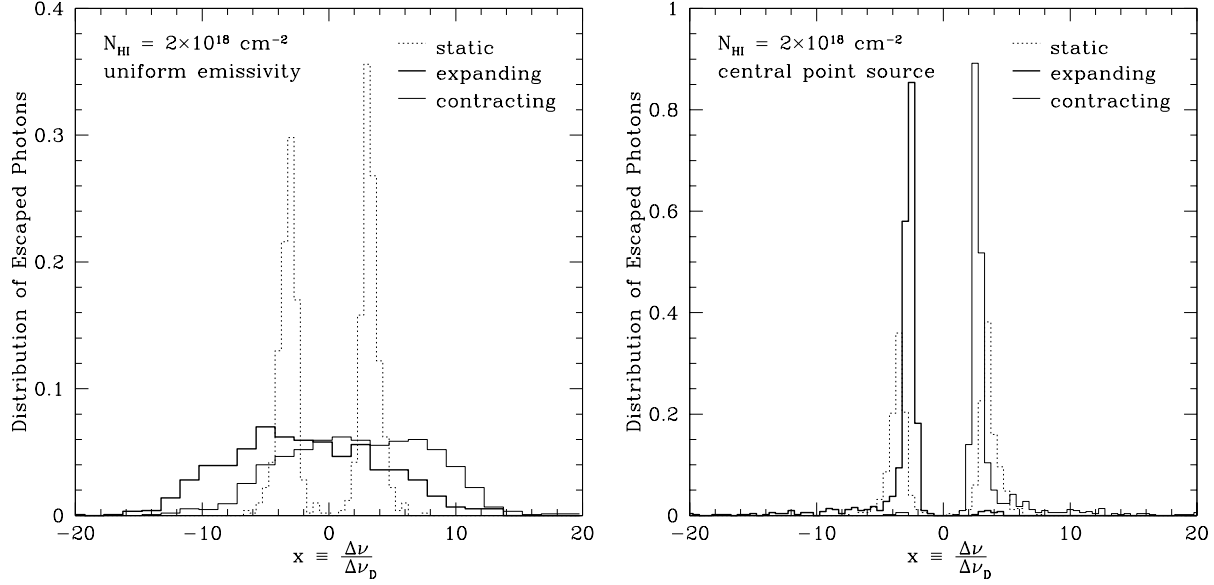


Fig. 2.— Frequency distribution of Ly α photons escaped from a uniform hydrogen cloud with neutral hydrogen column density $2 \times 10^{18} \text{ cm}^{-2}$ for the cases of uniform emissivity and central point source. Different line types are for a static, expanding, or contracting cloud.

Case 1: uniform emissivity, static cloud

Case 2: uniform emissivity, expanding or contracting cloud

Case 3: central point source, static cloud

Case 4: central point source, expanding or contracting cloud

For each case, we perform two runs with different column densities ($2 \times 10^{18} \text{ cm}^{-2}$ and $2 \times 10^{20} \text{ cm}^{-2}$). The temperature is assumed to be $2 \times 10^4 \text{ K}$ everywhere. In the case of expansion, we set it to be Hubble-like (i.e., the velocity is proportional to the radius), with the velocity at the edge of the system fixed to be 200 km s^{-1} . The cases of contraction are done in the same way; their line spectra can generally be obtained by simply mirror-reflecting in frequency the photons escaped from the expanding cloud about the rest frame Ly α frequency.

Figures 2 and 3 show the distribution of escaped photons for all the cases. For static cases, as expected, the escaped photons have a double-peaked frequency distribution. Except for the very small effect of atomic recoil (see Field 1959), the two peaks are exactly symmetric; the differences in the figures are due to the simulation noise.

To understand the results obtained, it is useful to think of the trajectory in frequency and space followed by a typical photon. In the case of a Lyman limit systems (like in Fig. 2), the photons are most likely to be scattered by atoms that have the right velocity along the photon

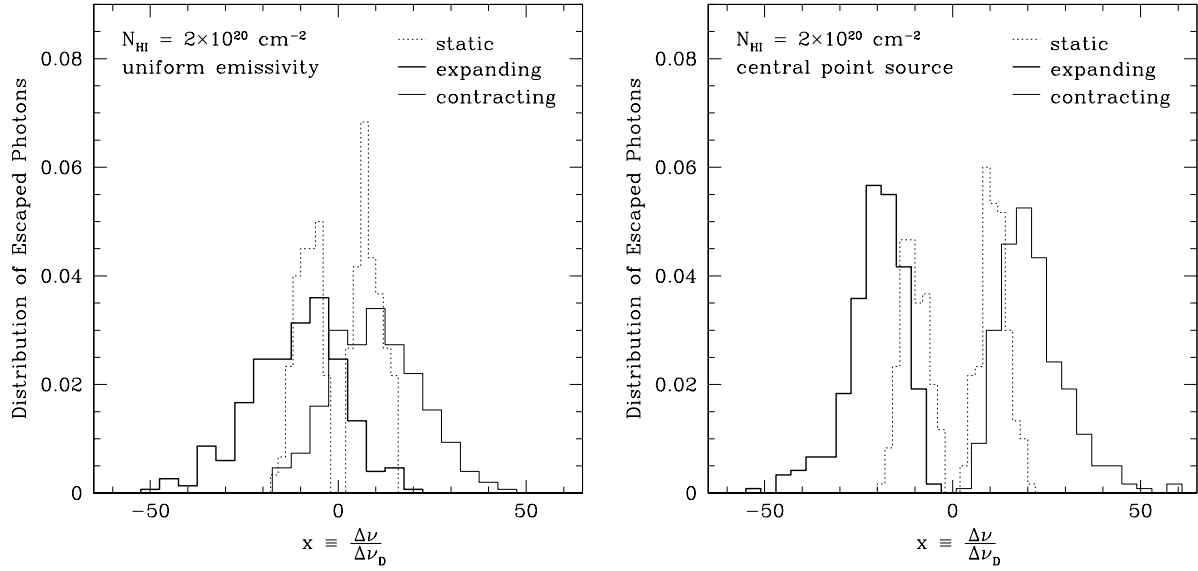


Fig. 3.— Same as Fig. 2, but for neutral hydrogen column density $2 \times 10^{20} \text{ cm}^{-2}$.

direction for shifting the photon frequency close to the line center in the atom frame. A photon is most likely to be found within a frequency range $\Delta\nu_D = (v_p/c)\nu_0$ of the line center, and will occasionally make larger excursions away from the line center when scattered by an atom having a large velocity perpendicular to the photon's direction. After any such excursion, the photon will likely return immediately to the line center with one or a few scatterings. Therefore, the photon escapes the cloud not by diffusing in frequency, but by a single large jump when scattered by an atom in the high-velocity tail of the Maxwellian distribution, which reduces its optical depth for escaping to a value of order unity. For a Lyman limit system with $N_{HI} = 2 \times 10^{18} \text{ cm}^{-2}$, the line-center optical depth is $\tau_0 = f_{12}\pi^{1/2}e^2N_{HI}/(m_e v_p \nu_0) = 8.3 \times 10^4$, and the photons escape when their optical depth is $\tau = \tau_0 e^{-x^2} \sim 1$ (where $x = \Delta\nu/\Delta\nu_D$), which implies $x \simeq \sqrt{\ln \tau_0} = 3.4$.

In the case of a DLA system, the scattering history differs from the Lyman limit case once the photon reaches a sufficiently large excursion in frequency to make it more likely that the next scattering is caused by a random atom far from the line center, rather than an atom moving with the right velocity to shift the photon frequency to the line center in the atom frame. Then, the evolution of the photon is described by diffusion in frequency. Since the photons are now reaching their escaping frequency not by a large jump but by a series of small steps, they undergo greater spatial diffusion than in Lyman limit systems. This, plus the fact that the optical depth has now a power-law instead of Gaussian dependence at large x , broadens the width of the two emission peaks. Of course, the emission peaks also move further from the line center because a smaller scattering cross section is required for the photons to escape.

In Figures 4 and 5, we can see that the surface brightness produced by a central point source

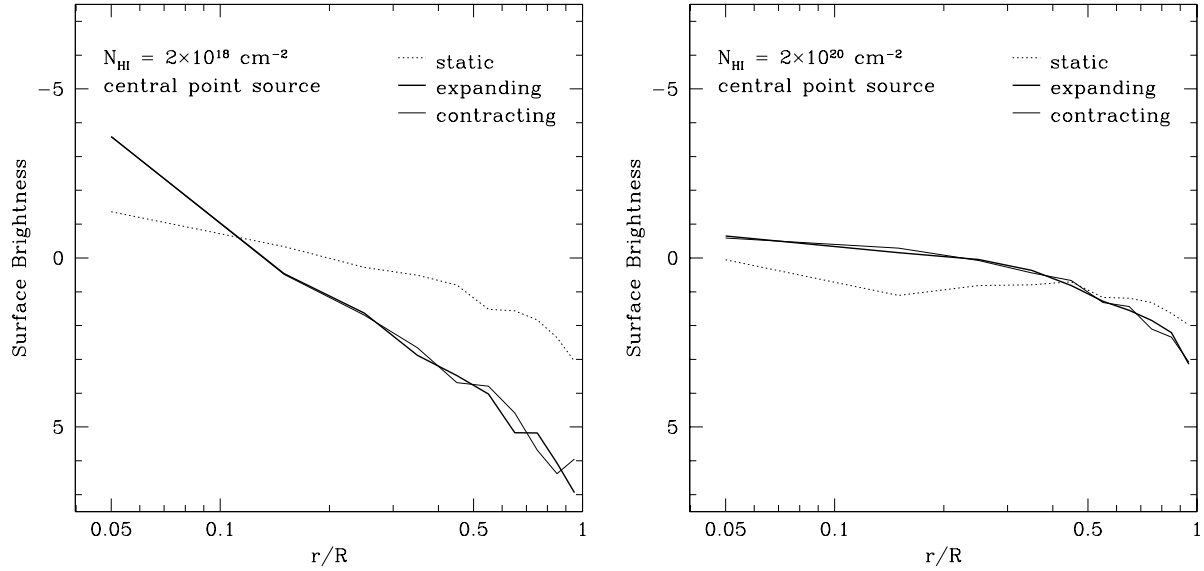


Fig. 4.— Surface brightness profiles, in magnitudes per solid angle (with an arbitrary zero point). Curves are normalized in such a way that the total energy of the photons remains the same. In the right panel, the drop at $r/R \sim 0.15$ for the static case is due to simulation noise.

is more extended for a DLA system than for a Lyman limit system, owing to the greater spatial diffusion.

For an expanding cloud, photons should escape with an average redshift because they are doing work on the expansion of the cloud as they are scattered. For a Lyman limit system with a central source, a photon undergoing a large positive frequency jump will be moved back to the line center relative to the fluid as it travels through the cloud, owing to the Hubble-like expansion of the cloud. On the other hand, a negative frequency jump will allow the photon to escape directly. In our case, the velocity at the cloud edge, 200 km s^{-1} , is much larger than the atomic velocity dispersion, so a photon needs to undergo many positive frequency jumps in order to diffuse spatially through the cloud and be able to escape on the blue side of the line, which explains why the blue peak is highly suppressed. The situation is exactly reversed for a contracting cloud. The case of uniform emissivity broadens the line, essentially because of the different velocities of the emission sites of the photons; there is also the additional effect that photons emitted near the edge of the cloud are more likely to escape on the blue (red) peak for an expanding (contracting) cloud. In DLAs, the line is also broader for a point source compared to a Lyman limit system because of the power-law dependence of the cross section on frequency and the greater degree of spatial diffusion.

To summarize, these simple models show how the frequency and spatial distributions of Ly α photons escaped from a cloud are related to the Ly α emissivity distribution, the bulk velocity field and the column density of the cloud.

4. Ly α Emission from Model Damped Ly α Systems

We now apply our code to a gas cloud with an isothermal density profile as a model for DLAs. The nature of DLAs is still a subject of debate. They could be protogalaxies with a rotating disk component (e.g., Prochaska & Wolfe 1997, 1998) or spherically distributed clouds of gas moving randomly in halos (e.g., Mo 1994; McDonald & Miralda-Escudé 1999). We investigate the emergent spectra and spatial distribution of the Ly α emission, to show what it can tell us about the internal structure of the system.

4.1. Model Description

We model the gas cloud producing a DLA assuming that it forms in a dark matter halo of mass $10^{11} M_{\odot}$, virialized at redshift $z = 3$. In an $\Omega_M = 1$ universe with $H_0 = 70 \text{ km s}^{-1} \text{Mpc}^{-1}$, the corresponding virial radius is $r_{\text{vir}} = 24 \text{ kpc}$, and the virial velocity $V_{\text{vir}} = 104 \text{ km s}^{-1}$ (e.g., Padmanabhan 1993). We assume the gas density profile is a singular isothermal sphere with a cutoff at the virial radius and a fraction of the halo mass in gas of 0.05.

We consider two different cases as an illustration to show how the rotation of a system could be probed by observations of Ly α emission. The first case is a spherically symmetric cloud, and the second a rotating oblate ellipsoid with an axis ratio of 0.5 for the gas distribution. The rotating velocity is set to be $V_{\text{rot}} = \sqrt{2/3}V_{\text{vir}}$. In one case, we assume the gas to be static and at a temperature $2 \times 10^4 \text{ K}$ (a typical temperature of gas that cools after shock-heating but stays photoionized). We also consider another case where the gas is given an additional velocity dispersion of $V_{\text{vir}}/\sqrt{3}$ in the spherical model, and $V_{\text{vir}}/3$ in the flattened, rotating model. This additional velocity dispersion is simply added quadratically to the thermal one, which would be valid if the gas were in optically thin clumps moving at this velocity dispersion. In practice, any relevant gas clumps in DLAs will be optically thick to Ly α photons, but their inclusion would make our model much more complex. We will discuss the effect we would expect from optically thick clumps in §5.

There are various sources to produce Ly α photons: internal dissipation and fluorescence caused by the intergalactic UV background. The external UV background will give rise to Ly α fluorescence; in an optically thick medium, recombination of the photoionized hydrogen has a 68% probability of producing a Ly α photon. Shock-heating of the gas will dissipate kinetic energy into heat, which will result in Ly α emission after line excitation and collisional ionization followed by recombination. In addition, internal star formation can of course also produce Ly α emission. We consider only fluorescent emission from the external background in this paper. For this kind of source, the emissivity is proportional to the square of the ionized gas density. The other two sources of emission are more centrally concentrated, and therefore similar differences as the ones between uniform emissivity and central source in the previous section can be expected.

We take self-shielding into account in the spherical case, calculating the neutral hydrogen

density of the cloud at every radius, where the total gas density profile is singular isothermal. We use an iterative algorithm similar to the one presented by Tajiri & Umemura (1998), as described in Zheng & Miralda-Escudé (2002). Here, we assume a UV background intensity of $10^{-22} \text{ ergs s}^{-1} \text{ cm}^{-2} \text{ s}^{-1} \text{ Hz}^{-1} \text{ sr}^{-1}$, constant at all frequencies between the H I Lyman limit, ν_L , and the He II Lyman limit, $4\nu_L$. The intensity is set to zero at frequencies above $4\nu_L$. The profile of neutral hydrogen that is obtained is similar to that shown in Zheng & Miralda-Escudé (2002). In the case of the flattened, rotating gas distribution, we simply take the same neutral hydrogen density profile as for the spherical case and flatten it with an axis ratio of 0.5 (the numerical code we have developed for computing the self-shielding correction applies only to spherically symmetric systems). This is of course not exact, although a much better approximation than neglecting self-shielding altogether.

4.2. Results of Simulations

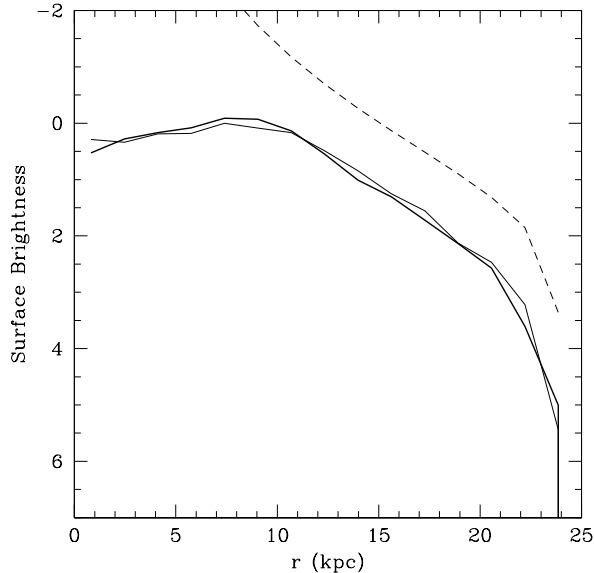


Fig. 5.— Surface brightness profiles of Ly α emission for the spherically symmetric cloud (in magnitudes per unit solid angle, with an arbitrary normalization). Thick and thin lines are with and without velocity dispersion, respectively (see the text). Dashed line is for optically thin cloud (with an arbitrary vertical shift)..

The surface brightness profile for the spherically symmetric, non-rotating cloud is plotted in Figure 5. The thick solid line shows the case of including the fluid velocity dispersion, $\sigma = V_{\text{vir}}/\sqrt{3} = 60 \text{ km s}^{-1}$, while the thin solid line is the result with only the thermal velocity dispersion, $(kT/m_H)^{1/2} = 12.8 \text{ km s}^{-1}$. The dashed line is what is obtained when self-shielding is not included. The velocity dispersion has practically no effect on the surface brightness profile, because the change

in spatial diffusion of the photons is very small. The emissivity due to the recombination has a “hole” in the inner part of the cloud because of self-shielding. Therefore, we see a “core” in the surface brightness profile (with a slight decline of surface brightness toward the center in the inner part due to geometric effects). The outer part of the profile follows the optically thin case. The core of the surface brightness profile is a signature that the emission is due to fluorescence of the external background, since other sources of emission are more centrally concentrated.

Because the ionizing photons of the external background extend only up to $4\nu_H$ in frequency (since higher frequency photons are absorbed by He II before reaching the hydrogen self-shielded zone), essentially all the photoionizations and subsequent recombinations occur in the outer region of the gas cloud with a hydrogen column density of $N_{HI} \lesssim 10^{19} \text{ cm}^{-2}$, the inverse of the photoionization cross section at frequency $4\nu_L$. The damped absorption wings are not yet important at this column density, therefore the photons escape the cloud after a single large jump in frequency when scattered by an atom in the high-velocity tail of the Maxwellian distribution, as discussed in §3 for the case of Lyman limit systems.

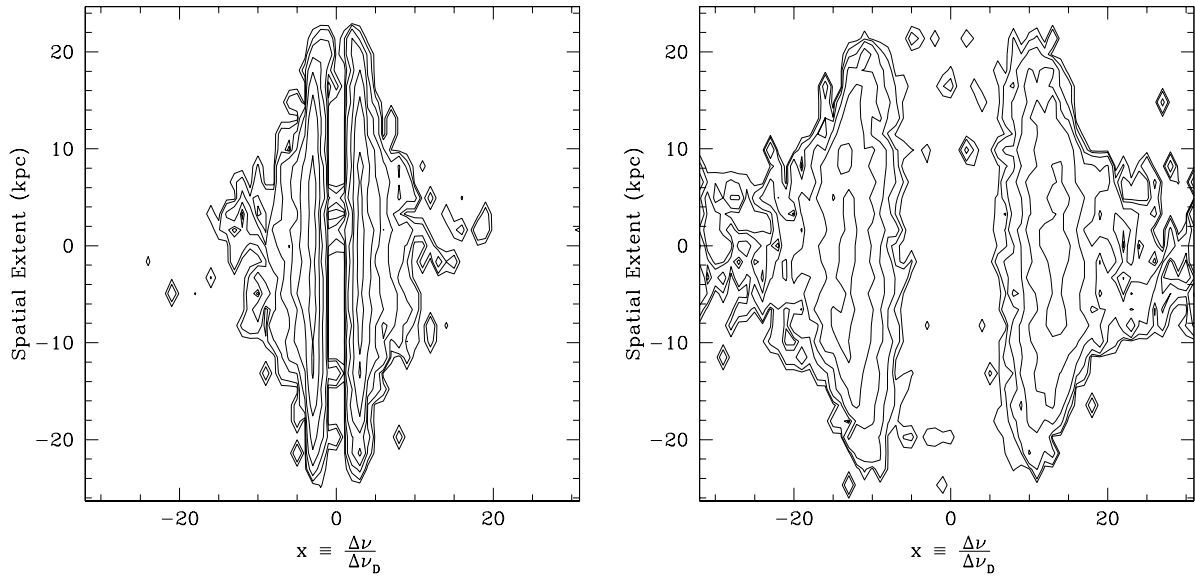


Fig. 6.— Two-dimensional spectra of spherically symmetric, non-rotating cloud. Left panel is for thermal velocity dispersion of $(kT/m_H)^{1/2} = 12.8 \text{ km s}^{-1}$ only, right panel includes a fluid velocity dispersion of 60 km s^{-1} (see the text).

Figure 6 shows the 2-dimensional spectra of the Ly α photons escaped from the non-rotating cloud. We assume that the slit is large enough to include the entire cloud. The double-peaked distribution of escaped Ly α photons, with the intermediate frequency range of essentially zero flux, appears at every spatial position.

Including an additional velocity dispersion has the effect of separating the two peaks. This is

true in our model because we consider the case where there is no correlation between the velocity of two atoms that are spatially close, valid only when any gas clumps moving coherently are so small that they are optically thin to Ly α photons. In other words, the additional velocity dispersion is effectively thermal. In the presence of coherent motions of optically thick regions, the intermediate frequency range with a highly reduced flux disappears, as discussed in §3 in the examples of an expanding or contracting cloud.

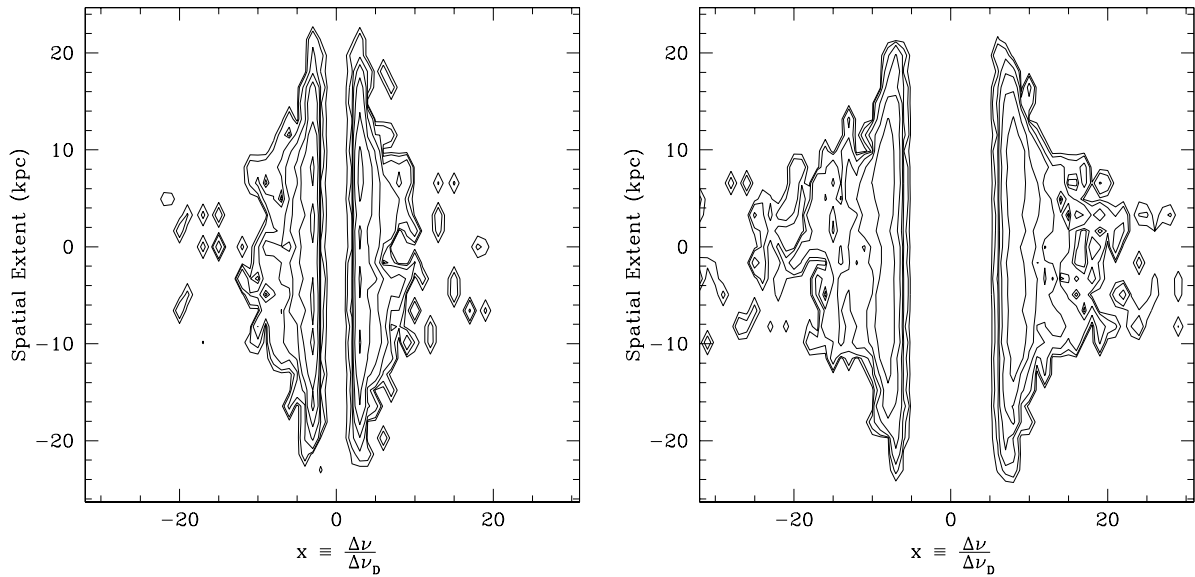


Fig. 7.— Two-dimensional spectra of the oblate rotating cloud viewed face-on. Left panel is for thermal velocity dispersion of 12.8 km s^{-1} only, right panel includes an additional velocity dispersion of 35 km s^{-1} (see the text).

Spectra of the flattened rotating cloud depend on the viewing angle and slit orientation. The face-on spectrum, plotted in Figure 7, is very similar to that of the spherical static case. Figure 8 shows the edge-on spectra, with the slit perpendicular (top panels) and parallel (bottom panels) to the rotational axis. The spectrum is averaged along the spatial coordinate perpendicular to the slit; in other words, we are assuming that the entire cloud is included in the slit, but that the wavelength dispersion is wide enough that the size of the cloud does not introduce any smoothing of the spectrum. When the slit is perpendicular to the rotation axis, the rotation curve pattern is clearly seen. The velocity shift of the spectrum is about the same as the rotational velocity, $V_{\text{rot}} = V_{\text{vir}}\sqrt{2/3} = 85 \text{ km s}^{-1}$, at the edge of the system [note that the unit used in the horizontal axis is $\Delta\nu_D = (2kT/m_H)^{1/2}\nu_0/c = 18.2 \text{ km s}^{-1}(\nu_0/c)$]. The variation of the shape of the spectrum along the slit is easily understood by thinking of an analogy to the expanding and contracting cloud in §3. The Ly α photons are produced on the outer ionized layer of the system, near the radius r_{ss} where the hydrogen becomes self-shielding. The line-of-sight velocity at this radius is proportional to $V_{\text{rot}}r_p/r_{\text{ss}}$, where r_p is the projected radius on the slit position. Therefore, the central trough

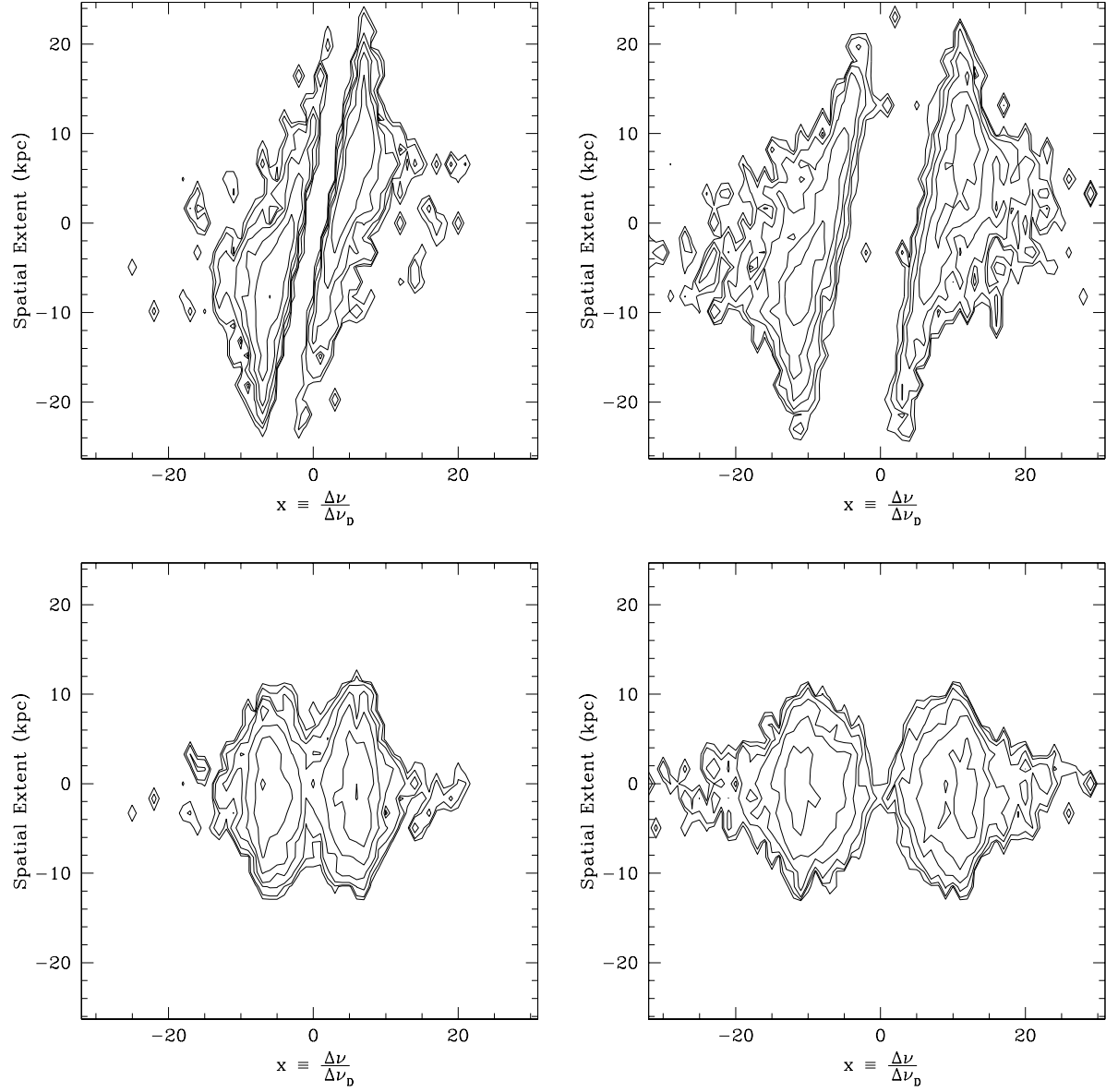


Fig. 8.— Two-dimensional spectra of oblate rotating cloud viewed edge-on, with the slit perpendicular (top panels) and parallel (bottom panels) to the rotation axis. Left and right panels are for cases of different velocity dispersions as explained in Fig. 7.

of the spectrum shifts linearly with the projected radius. Moreover, the variation of the velocity along the line of sight causes the peak of emission that is further from the mean velocity of the system to be enhanced, for similar reasons as in the case of the expanding and contracting clouds discussed in §3.

For the case of the slit parallel to the rotational axis, the 2-dimensional spectrum displays a symmetric double-peaked pattern, which essentially results from averaging along the equator the spectrum with different projected velocity. This averaging results in a less sharp central trough and smoothing of the two peaks. In all cases, the velocity dispersion increases the distance between the two peaks in the photon distribution and broadens the width of each peak.

5. Summary and Discussion

We have developed a Monte Carlo code of Ly α photon scattering, to construct simulated images and spectra. The code is fully three-dimensional and adaptable to a cloud with any given Ly α emissivity, neutral hydrogen density distribution, and bulk velocity field. Several simple cases have been presented to show the images and spectra expected from a uniform gas distribution. We have applied the code to model DLA systems illuminated by the intergalactic UV background to study the spatial and frequency distribution of emitted Ly α photons. Self-shielding produces a core in the Ly α surface brightness profile. For a spherical, static cloud, Ly α photons have a double-peaked distribution which is symmetric around the line center frequency. An oblate, rotating cloud shows the same double-peak distribution with the rotational pattern of increasing mean wavelength with the position on the slit. Observations of the fluorescent emission from damped Ly α systems with large telescopes (Hogan & Weymann 1987; Gould & Weinberg 1996) could reveal the presence of such systems and measure a velocity gradient, providing a direct measurement of the rotation rate. The Ly α image would also reveal if the emission is due to fluorescence from the external radiation (in which case we expect a large core of the surface brightness at the radius where the hydrogen becomes self-shielded) or due to internal gas dissipation or star formation.

The observations of metal lines in DLA systems show multiple absorption lines (e.g., Prochaska & Wolfe 1997, 1998), suggesting that the gas is clumpy. In this paper, we have assumed instead that the gas has a smooth distribution. The case of enhanced velocity dispersion we have considered is valid only if the gas is in very small clumps that are optically thin to Ly α photons. Clumps that can give rise to the observed metal lines are highly optically thick. The effect of a clumpy gas distribution is not difficult to imagine. If there is only one clump along a line of sight, then this clump will essentially produce the same spectral shape in its emission line, shifted to its velocity. Thus, if the emission line could be observed with sufficient angular resolution to resolve the individual clumps, the characteristic spectral shape of Figure 6 would appear at every position, although shifted to the clump velocity. If the clumps are not resolved, the emission line shape is obviously smoothed, just like in the case of an expanding or contracting cloud shown in Figure 2. Our numerical code can be applied in the future to the results of detailed hydrodynamic simulations of gaseous halos in

the process of forming galaxies in cosmological realizations to predict other observable signatures that can test the mechanisms by which energy dissipation of gas leads to galaxy formation.

We thank Xuelei Chen and David Weinberg for useful discussions. This work was supported in part by NSF grant NSF-0098515.

REFERENCES

Adams, T. F. 1972, *ApJ*, 174, 439

Ahn, S.-H., Lee H.-W., & Lee, H.-M. 2000, *JKAS*, 33, 29

Ahn, S.-H., Lee H.-W., & Lee, H.-M. 2001, *ApJ*, 554, 604

Ahn, S.-H., Lee H.-W., & Lee, H.-M. 2001, *ApJ*, 567, 922

Bonilha, J. R. M., Ferch, R., Salpeter, E. E., Slater, G., & Noerdlinger, P. D. 1979, *ApJ*, 233, 649

Briggs, F. H., Wolfe, A. M., Liszt, H. S., Davis, M. M., & Turner, K. C. 1989, *ApJ*, 341, 650

Djorgovski, S. G., Pahre, M. A., Bechtold, J., & Elston, R. 1996, *Nature*, 382, 234

Field, G. 1959, *ApJ*, 129, 551

Gould, A., & Weinberg, D. H. 1996, *ApJ*, 468, 462

Harrington, J. P. 1973, *MNRAS*, 162, 43

Harrington, J. P. 1974, *MNRAS*, 166, 373

Haardt, F., & Madau, P. 1996, *ApJ*, 461, 20

Hogan, C. J., & Weymann, R. J. 1987, *MNRAS*, 225, P1

Hummer, D. G., & Kunasz, P. B. 1980, *ApJ*, 236, 609

Lu, L., Sargent, W. L. W., Barlow, T. A., Churchill, C. W., & Vogt, S. S. 1996, *ApJS*, 107, 475

McDonald, P., & Miralda-Escudé, J. 1999, *ApJ*, 519, 486

Mo, H. J. 1994, *MNRAS*, 269, L49

Neufeld, D. A. 1990, *ApJ*, 350, 216

Padmanabhan, T. 1993, *Structure Formation in the Universe* (Cambridge: Cambridge Univ. Press)

Prochaska, J. X., & Wolfe, A. M. 1997, *ApJ*, 487, 73

Prochaska, J. X., & Wolfe, A. M. 1998, ApJ, 507, 113

Prochaska, J. X., Gawiser, E., & Wolfe, A.M. 2001, ApJ, 552, 99

Tajiri, Y., & Umemura, M. 1998, ApJ, 502, 59

Zheng, Z., & Miralda-Escudé, J. 2002, ApJ, 568, L71